

# Cascaded metasurface for separated information encryption [Invited]

Jiahao Wang (汪嘉豪)<sup>1</sup>, Guodong Zhu (朱国栋)<sup>2</sup>, Weiguo Zhang (张为国)<sup>2\*</sup>, Zhou Zhou (周舟)<sup>1</sup>, Zile Li (李子乐)<sup>1,3</sup>, and Guoxing Zheng (郑国兴)<sup>1,3,4\*\*</sup>

<sup>1</sup>Electronic Information School, Wuhan University, Wuhan 430072, China

<sup>2</sup>Chongqing Institute of Green and Intelligent Technology, Chinese Academy of Sciences, Chongqing 400714, China

<sup>3</sup>Peng Cheng Laboratory, Shenzhen 518055, China

<sup>4</sup>Wuhan Institute of Quantum Technology, Wuhan 430206, China

\*Corresponding author: [zwg@cigit.ac.cn](mailto:zwg@cigit.ac.cn)

\*\*Corresponding author: [gxzheng@whu.edu.cn](mailto:gxzheng@whu.edu.cn)

Received October 15, 2022 | Accepted December 16, 2022 | Posted Online February 24, 2023

For a conventional cascaded metasurface, the combination channel and each single channel are mutually dependent because the phase modulation of a cascaded metasurface is the sum of each single one. Here we propose a cascaded metasurface that can independently encode information into multiple channels. Based on the orientation degeneracy of anisotropic metasurfaces, each single metasurface can produce a quick-response (QR) image in the near field, governed by the Malus law, while the combined channel can produce a holographic image in the far field, governed by geometric phase. The independent and physically separated trichannel design makes information encryption safer.

**Keywords:** cascaded metasurfaces; optical encryption; holography; nanoprinting.

**DOI:** [10.3788/COL202321.020003](https://doi.org/10.3788/COL202321.020003)

## 1. Introduction

Metasurfaces<sup>[1–5]</sup>, ultrathin optical elements composed of subwavelength antenna arrays, have exhibited unprecedented wavefront modulation properties by imposing individual phase and/or amplitude shifting. Benefiting from their flexibility in wavefront manipulation, a large variety of optical metasurface-based devices have been demonstrated for various functionalities, such as metalenses<sup>[6–9]</sup>, vortex beam generators<sup>[10,11]</sup>, full-Stokes polarization cameras<sup>[12]</sup>, and ultracompact image displays, including holography<sup>[13,14]</sup> and nanoprinting<sup>[15,16]</sup>. Regarding metasurface holography, a series of novel multiplexing schemes have been proposed to improve information capacity and information security recently, where different holographic images are encoded along multiple optical dimensions<sup>[17–23]</sup>. However, conventional metasurface multiplexing techniques are based on single-layer frameworks, which allows for distinct encrypted information displayed in different channels. Since the separation of information in physical space is ignored, one must face a situation where once the medium on which the information is stored has been accessed, all information is at risk of exposure. In this context, multilayer metasurface frameworks offer an alternative for the physical separation of layers and the inherent information that can enhance the security of information.

Recently, some research works based on multiple phase profiles have been reported for optical encryption<sup>[24–27]</sup>. Among them, cascading metasurfaces along the propagation direction provide a high-security way for optical encryption, since each single metasurface can be physically separated and the secret can be shared to each single one. For example, Georgi *et al.* proposed a strategy that divides information storage metasurfaces into two categories; any piece of these categories can be cascaded with any piece of the other category to produce a designed hologram<sup>[25]</sup>. Wei *et al.* proposed in-plane rotation cascaded metasurfaces: by changing the relative rotation angles between cascaded metasurfaces, different holograms can be generated<sup>[26]</sup>. Zhou *et al.* proposed step-moving cascaded metasurfaces by changing the distance between the cascaded metasurfaces, resulting in different holograms in the target plane<sup>[27]</sup>. These strategies can achieve the separation of information in physical space. However, because the phase modulation of a cascaded metasurface is the sum of each single metasurface, the combination channels and each single metasurface channel are mutually dependent, which therefore lowers the information capacity of each channel and leads to unwanted cross talk.

In this Letter, we propose a new strategy for cascaded metasurface design, in which each single metasurface is governed by amplitude control used for nanoprinting while their

combination channel is governed by geometric phase control used for holography. Since amplitude and phase are independently controlled corresponding to different channels, the combination channel and each single metasurface channel become mutually independent. Therefore, by dividing the information into the two different image display platforms, not only can the information capacity of each channel reach its maximum, but also the information storage and delivery become safer, since the information of different channels is decrypted with different optical setups.

## 2. Principle

As shown in Fig. 1, the working principle of the proposed cascaded metasurface with three independent channels can be described as follows. Two pieces of metasurfaces form the main framework of the multichannel information encryption system. Each of them contains an encrypted nanoprinting image, and the image can be constructed upon the action of meta-key 1, which provides the illumination with  $x$ -polarized light, filtered with a horizontal analyzer. These nanoprinting images float right above the metasurface plane and serve as a unique identifier for each metasurface. Meanwhile, two metasurfaces can reconstruct an encrypted Fourier holographic image in the far field upon the action of meta-key 2, which provides the illumination of circularly polarized light when two metasurfaces are strictly aligned, as shown at the right of Fig. 1. This holographic image can be used as encrypted information that is only revealed if both metasurfaces have that particular identifier. In our design, the metasurface 1 will display a QR code that contains the longitude value of our laboratory, and the metasurface 2 will display another QR code that contains the latitude value of our laboratory; the holographic image shows the room number of our laboratory.

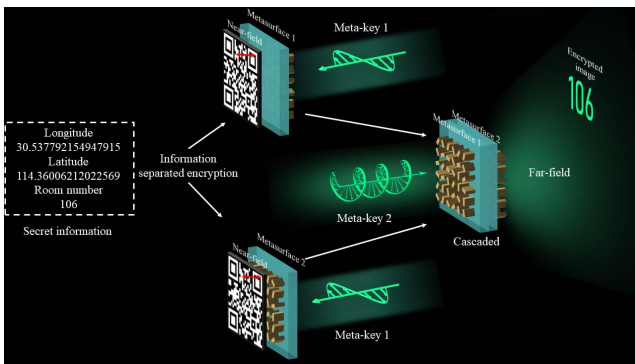


**Fig. 1.** Schematic diagram of the proposed separated information encryption via a cascaded metasurface. The secret information is divided into two metasurfaces; each one of the two metasurfaces contains the information of a nanoprinting image and part of a holographic image. The individual nanoprinting image of each single metasurface is decoded in the near field, under the action of meta-key 1. The holographic image is decoded in the far field under the action of meta-key 2 when the two metasurfaces are cascaded.

To achieve the above-mentioned physical separation of information encryption, dielectric nanobricks acting as nano-half-wave plates are employed to record three independent images. We first consider the amplitude modulation of a nano-half-wave plate placed in the parallel-polarization optical path, which corresponds to the working channel of a single metasurface. As shown in Fig. 2(a), the incident light propagates along the  $z$  axis and passes in turn through an  $x$  polarizer; the metasurface has an orientation angle  $\theta$  relative to the  $x$  axis and the  $x$ -analyzer. The Jones vector of output light can be expressed as

$$\begin{aligned} T(\theta) &= J_a R(-\theta) J_{\text{hp}} R(\theta) E_{\text{in}} \\ &= \begin{bmatrix} 1 & 0 \\ 0 & 0 \end{bmatrix} \begin{bmatrix} \cos \theta & -\sin \theta \\ \sin \theta & \cos \theta \end{bmatrix} \\ &\quad \cdot \begin{bmatrix} 1 & 0 \\ 0 & -1 \end{bmatrix} \begin{bmatrix} \cos \theta & \sin \theta \\ -\sin \theta & \cos \theta \end{bmatrix} \begin{bmatrix} 1 \\ 0 \end{bmatrix} \\ &= \begin{bmatrix} \cos 2\theta \\ 0 \end{bmatrix}, \end{aligned} \quad (1)$$

where  $J_a$  is the Jones matrix of  $x$ -analyzer,  $J_{\text{hp}}$  is the Jones matrix of nano-half-wave plate,  $E_{\text{in}}$  is the Jones vector of the incident light, and  $\theta$  is the orientation angle of each nano-half-wave plate. Based on Eq. (1), the intensity of output light can be expressed as

$$I(\theta) = I_0 \cos^2 2\theta, \quad (2)$$

where  $I_0$  is the incident light intensity. Based on Eq. (2), there are four orientation angles that can produce an equal output light

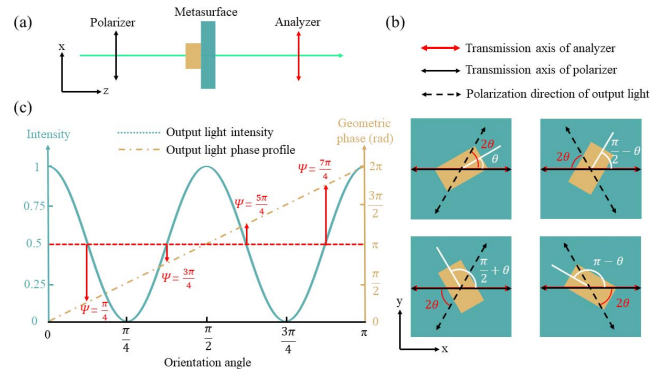


**Fig. 2.** Working principles of cascaded metasurfaces for separated encryption. (a) Working optical path to encrypt the nanoprinting image; the black and red two-way arrows represent the polarization direction of polarizer and analyzer, respectively, and the incident light propagates along the  $z$  axis. (b) Orientation distribution generating the equal output light intensity; (c) curves for the output intensity and the generated geometric phase by metasurfaces with different orientation angles; for a given optical intensity, there are four orientation choices to generate different geometric phases. As an example, the intersections of the red dashed line and the output light intensity curve represent for the same output light intensity 0.5, but different output light phase profiles. The output light phase profiles can be chosen to be  $\pi/4$ ,  $3\pi/4$ ,  $5\pi/4$ , or  $7\pi/4$ .

intensity due to the orientation degeneracy of anisotropic metasurfaces<sup>[15]</sup>. As shown in Fig. 2(b), when the orientation angle of the nano-half-wave plate turns into  $\pi/2 - \theta$ ,  $\pi/2 + \theta$ , or  $\pi - \theta$ , the intensity of output light equals the situation in which the orientation angle of the nano-half-wave plate is set to be  $\theta$ , and the angles between output lights and analyzer are  $2\theta$ . Benefiting from the new degrees of freedom suggested by the orientation degeneracy, the metasurface can produce different geometric phases of incident light with the same output light intensity. Geometric phase, known also as the Pancharatnam–Berry phase, can be utilized to produce a phase delay that is exactly twice the orientation angle of the metasurface. Four nano-half-wave plates are rotated at four different orientation angles, and they can produce the equal output light intensity but different geometric phases for circularly polarized output light with opposite rotation:  $2\theta$ ,  $\pi - 2\theta$ ,  $\pi + 2\theta$ ,  $2\pi - 2\theta$  to left-handed circularly polarized (LCP) light incidence. If the incident light is changed to be right-handed circularly polarized (RCP), the sign of the geometric phase will be reversed, but the value of the geometric phase delay will be constant. To better understand the relationship between the intensity modulation and the geometric phase modulation of the nano-half-wave plate, the curves of output light intensity and geometric phase variation with the orientation angle of nano-half-wave plate are shown in Fig. 2(c).

Based on the geometric phase modulation of the metasurface, the normally incident LCP light propagates through the first metasurface with an orientation angle  $\theta_1$ ; LCP light will be transformed into RCP light, and the RCP light propagating through the second metasurface with an orientation angle  $\theta_2$  will be transformed into LCP light. With two metasurfaces strictly aligned, the phase delay attached to output LCP can be expressed as

$$E_{\text{out}} = e^{i(2\theta_1 - 2\theta_2)} E_{\text{in}}, \quad (3)$$

where  $E_{\text{in}}$  and  $E_{\text{out}}$  are the Jones vectors of incidence and output LCP, respectively. Based on Eq. (3), we can modulate the output LCP phase delay pixel-by-pixel by rotating the orientation angles of the metasurfaces.

Figure 3 diagrams the orientation angles selection algorithm of our design strategy, and the orientation angles design principles are to minimize the different values between the phase delay attached to the output LCP and the phase delay obtained by Gerchberg–Saxton (GS) algorithm. For the designed target image 1 and target image 2 encrypted in metasurface 1 and metasurface 2, the orientation angles distribution of the two metasurfaces can be calculated by Eq. (2). Due to the orientation degeneracy, the orientation angle of each pixel on the metasurface has four choices. The output LCP phase distribution can be calculated by Eq. (3), and by changing the combination of  $\theta_1$  and  $\theta_2$ , we can get 16 kinds of phase delay  $\Psi_{\text{sum}}$  attached on the output LCP light. Figure 3 has shown the traversal method applied in the algorithm. The phase distribution  $\varphi$  of the target holographic image can be obtained by the GS algorithm, which has been widely applied in holographic image design. The next step is to choose the proper  $\Psi_1$  and  $\Psi_2$  to minimize the

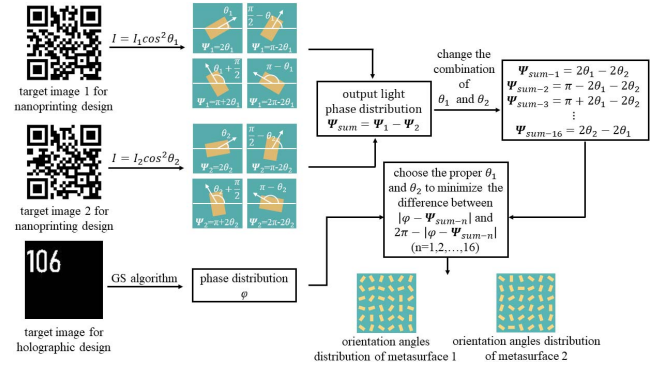


Fig. 3. Flow chart of designing cascaded metasurfaces for separated information encryption. Combining the orientation degeneracy and geometric phase, different information can be encrypted into different working channels and different metasurfaces.

difference value between  $\varphi$  and  $\Psi_{\text{sum}-n}$  ( $n = 1, 2, \dots, 16$ ). In this way, we can obtain the orientation angle distribution of metasurface 1 and metasurface 2, respectively.

Figure 4(a) shows the diagram of an individual unit-cell nanostructure. The nanostructure is composed of a  $\text{TiO}_2$  nanobrick and a  $\text{SiO}_2$  substrate. The cell size of unit cell is set to be  $C = 400$  nm and the height of the nanobrick is set to be  $H = 600$  nm; the gap between two metasurfaces is set to be 600 nm. In order to optimize the parameters of the nanobrick to make it exhibit as a half-wave plate, transmission coefficients along the long and short axes of the nanobricks are simulated by FDTD Solutions at a fixed working wavelength of 532 nm. Figures 4(b)–4(d) show the simulation results, and the sizes of the nanobrick are ultimately chosen to be  $L = 180$  nm and  $W = 100$  nm.

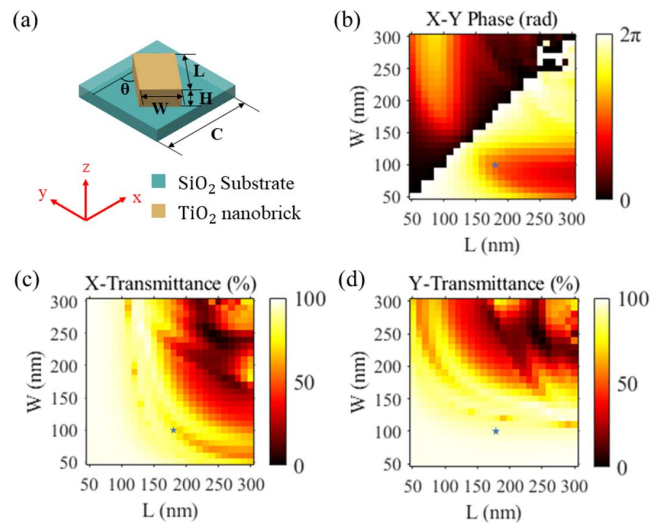
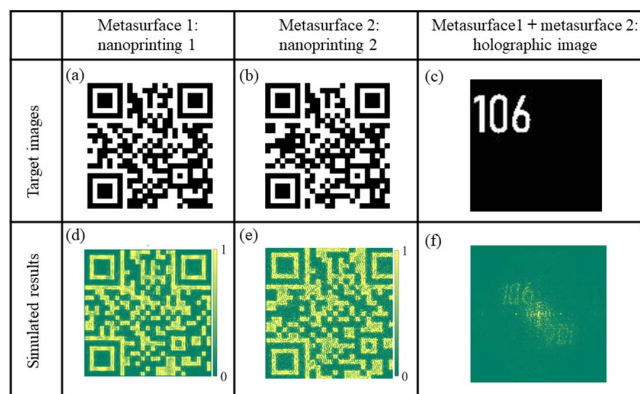


Fig. 4. Illustration of a unit-cell of a cascaded metasurface and the numerically simulated optical response. (a) Schematic of a unit-cell structure with a  $\text{TiO}_2$  nanobrick and a  $\text{SiO}_2$  substrate; (b) simulated phase delays between the long and short axes of the nanobrick; (c), (d) simulated transmittances under the illumination of  $x$ - and  $y$ -polarized incident light. The optimally selected nanobrick parameters are marked with a blue star.



**Fig. 5.** The target images and simulation results of separated information encryption. (a)–(c) The target images are set to be 120 pixels  $\times$  120 pixels. (d)–(f) Simulated results of nanoprinting images and holographic image.

In our design, the target images for nanoprinting are two QR codes that contain the longitude and latitude values of our laboratory, and the target image for hologram is the room number of our laboratory. In the simulation of reconstructing a holographic image, two metasurfaces are set to be strictly aligned and tightly fit on the substrate. Each metasurface is composed of 120 pixels  $\times$  120 pixels. The near-field nanoprinting patterns are obtained by a monitor set at a distance of one wavelength from the surface of metasurface 2, and the far-field holographic image is obtained by the ‘farfield’ function in the monitor set at the surface of metasurface 2. As a result, the simulation results are shown in Fig. 5. It can be seen, under the illumination of  $x$ -polarized incident light at the wavelength of 532 nm, two metasurfaces can reconstruct the designed QR codes. Under the illumination of LCP light at the wavelength of 532 nm, the cascaded metasurfaces can reconstruct the holographic image ‘106’ in the far field. Therefore, all simulation results agree well with the target patterns.

### 3. Conclusion

In summary, we propose cascaded metasurfaces for independent and separated information encryption. Two metasurfaces composed of  $\text{TiO}_2$  nano-half-wave plates are encoded to display two individual nanoprinting images under a parallel-polarization optical path. With their combination, a holographic image is displayed in the far field under the illumination of CP light. Encrypted information is encoded into different working channels and different metasurfaces and can be decrypted under different observation conditions. The proposed design method provides a safer way for metasurface encryption, which can be used in optical encryption, watermarking, and anticounterfeiting with a high security level.

### Acknowledgement

This work was supported by the National Key Research and Development Program of China (No. 2021YFE0205800), the

National Natural Science Foundation of China (Nos. 12174292, 11904267, and 91950110), and the Fundamental Research Funds for the Central Universities (Nos. 2042022kf1013, 2042022kf0024, and 2042021kf0018).

### References

- W. Ma, Y. Xu, B. Xiong, L. Deng, R. W. Peng, M. Wang, and Y. Liu, “Pushing the limits of functionality-multiplexing capability in metasurface design based on statistical machine learning,” *Adv. Mater.* **34**, 2110022 (2022).
- S. Krasikov, A. Tranter, A. Bogdanov, and Y. Kivshar, “Intelligent metaphotonics empowered by machine learning,” *Opto-Electron. Adv.* **5**, 210147 (2022).
- Q. Song, M. Odeh, J. Zuniga, B. Kante, and P. Genevet, “Plasmonic topological metasurface by encircling an exceptional point,” *Science* **373**, 1133 (2021).
- Z. Cai and Y. Liu, “Near-infrared reflection modulation through electrical tuning of hybrid graphene metasurfaces,” *Adv. Opt. Mater.* **10**, 2102135 (2022).
- S. Iqbal, H. Rajabalipanah, L. Zhang, X. Qiang, A. Abdolali, and T. J. Cui, “Frequency-multiplexed pure-phase microwave meta-holograms using bispectral 2-bit coding metasurfaces,” *Nanophotonics* **9**, 703 (2020).
- W. T. Chen, A. Y. Zhu, V. Sanjeev, M. Khorasaninejad, Z. Shi, E. Lee, and F. Capasso, “A broadband achromatic metalens for focusing and imaging in the visible,” *Nat. Nanotechnol.* **13**, 220 (2018).
- S. Wang, C. P. Wu, V. C. Su, Y. C. Lai, M. K. Chen, H. Y. Kuo, B. H. Chen, H. Chen, Y. T. T. Huang, J. H. Wang, R. M. Lin, C. H. Kuan, T. Li, Z. Wang, S. Zhu, and D. P. Tsai, “A broadband achromatic metalens in the visible,” *Nat. Nanotechnol.* **13**, 227 (2018).
- E. Arbabi, A. Arbabi, S. M. Kamali, Y. Horie, M. Faraji-Dana, and A. Faraon, “MEMS-tunable dielectric metasurface lens,” *Nat. Commun.* **9**, 812 (2018).
- Y. Cui, G. Zheng, M. Chen, Y. Zhang, Y. Yang, J. Tao, T. He, and Z. Li, “Reconfigurable continuous-zoom metalens in visible band,” *Chin. Opt. Lett.* **17**, 111603 (2019).
- L. Deng, Z. Li, Z. Zhou, Z. He, Y. Zeng, G. Zheng, and S. Yu, “Bilayer-metasurface design, fabrication, and functionalization for full-space light manipulation,” *Adv. Opt. Mater.* **10**, 2102179 (2022).
- Y. Bao, J. Ni, and C. W. Qiu, “A minimalist single-layer metasurface for arbitrary and full control of vector vortex beams,” *Adv. Mater.* **32**, 1905659 (2020).
- N. A. Rubin, G. D’Aversa, P. Chevalier, Z. Shi, W. T. Chen, and F. Capasso, “Matrix Fourier optics enables a compact full-Stokes polarization camera,” *Science* **365**, eaax1839 (2019).
- G. Zheng, H. Mühlenbernd, M. Kenney, G. Li, T. Zentgraf, and S. Zhang, “Metasurface holograms reaching 80% efficiency,” *Nat. Nanotechnol.* **10**, 308 (2015).
- J. Li, Y. Wang, C. Chen, R. Fu, Z. Zhou, Z. Li, G. Zheng, S. Yu, C. W. Qiu, and S. Zhang, “From lingering to rift: metasurface decoupling for near- and far-field functionalization,” *Adv. Mater.* **33**, 2007507 (2021).
- L. Deng, J. Deng, Z. Guan, J. Tao, Y. Chen, Y. Yang, D. Zhang, J. Tang, Z. Li, Z. Li, S. Yu, G. Zheng, H. Xu, C. W. Qiu, and S. Zhang, “Malus-metasurface-assisted polarization multiplexing,” *Light Sci. Appl.* **9**, 101 (2020).
- J. Deng, L. Deng, Z. Guan, J. Tao, G. Li, Z. Li, Z. Li, S. Yu, and G. Zheng, “Multiplexed anticounterfeiting meta-image displays with single-sized nanostructures,” *Nano Lett.* **20**, 1830 (2020).
- L. Huang, H. Mühlenbernd, X. Li, X. Song, B. Bai, Y. Wang, and T. Zentgraf, “Broadband hybrid holographic multiplexing with geometric metasurfaces,” *Adv. Mater.* **27**, 6444 (2015).
- K. T. Lim, H. Liu, Y. Liu, and J. K. Yang, “Holographic colour prints for enhanced optical security by combined phase and amplitude control,” *Nat. Commun.* **10**, 25 (2019).
- P. Zheng, Q. Dai, Z. Li, Z. Ye, J. Xiong, H. C. Liu, G. Zheng, and S. Zhang, “Metasurface-based key for computational imaging encryption,” *Sci. Adv.* **7**, eabg0363 (2021).
- J. Li, S. Kamin, G. Zheng, F. Neubrech, S. Zhang, and N. Liu, “Addressable metasurfaces for dynamic holography and optical information encryption,” *Sci. Adv.* **4**, eaar6768 (2018).

21. F. Yue, C. Zhang, X. F. Zang, D. Wen, B. D. Gerardot, S. Zhang, and X. Chen, "High-resolution grayscale image hidden in a laser beam," *Light Sci. Appl.* **7**, 17129 (2018).
22. H. Ren, G. Briere, X. Fang, P. Ni, R. Sawant, S. Héron, S. Chenot, S. Vézian, B. Damilano, V. Brändli, S. A. Maier, and P. Genevet, "Metasurface orbital angular momentum holography," *Nat. Commun.* **10**, 2986 (2019).
23. X. Fang, H. Ren, and M. Gu, "Orbital angular momentum holography for high-security encryption," *Nat. Photonics* **14**, 102 (2020).
24. G. Qu, W. Yang, Q. Song, Y. Liu, C. W. Qiu, J. Han, D. P. Tsai, and S. Xiao, "Reprogrammable meta-hologram for optical encryption," *Nat. Commun.* **11**, 5484 (2020).
25. P. Georgi, Q. Wei, B. Sain, C. Schlickriede, Y. Wang, L. Huang, and T. Zentgraf, "Optical secret sharing with cascaded metasurface holography," *Sci. Adv.* **7**, eabf9718 (2021).
26. Q. Wei, L. Huang, R. Zhao, G. Geng, J. Li, X. Li, and Y. Wang, "Rotational multiplexing method based on cascaded metasurface holography," *Adv. Opt. Mater.* **10**, 2102166 (2022).
27. H. Zhou, X. Li, H. Wang, S. Zhang, Z. Su, Q. Jiang, N. Ullah, X. Li, Y. Wang, and L. Huang, "Ultra-dense moving cascaded metasurface holography by using a physics-driven neural network," *Opt. Express* **30**, 24285 (2022).